Polymer Journal (2017) 49, 189–195
© 2017 The Society of Polymer Science, Japan (SPSJ) All rights reserved 0032-3896/17
www.nature.com/pj

ORIGINAL ARTICLE

Supramolecular polymerization of hydrogen-bonded rosettes with anthracene chromophores: regioisomeric effect on nanostructures

Deepak D Prabhu, Keisuke Aratsu, Mitsuaki Yamauchi, Xu Lin, Bimalendu Adhikari and Shiki Yagai

Two regioisomeric barbituric acid compounds possessing (phenylethynyl) anthracene cores and tridodecyloxy phenyl units were synthesized. UV–Vis spectroscopic studies showed that the two compounds self-assemble by a cooperative mechanism in methylcyclohexane (MCH) with different stacking arrangements of the π-conjugated core, which leads to distinct aggregation-induced color changes. Atomic Force Microscopic studies revealed the formation of well-defined fibrous supramolecular polymers with different topological features, that is, cylindrical or helically twisted shapes. For the helically twisted supramolecular polymer, adding small amounts of limonene as a cosolvent induced more pronounced changes in absorption, which indicated an increased π–π stacking interaction in the cosolvent system compared with that in pure MCH. Molecular modeling studies suggested that the two molecules form supramolecular polymers by forming hydrogen-bonded hexameric supermacrocycles (rosettes) and that different twisting angles of the anthracene chromophore with respect to the barbituric acid plane can explain the observed difference in spectroscopic and morphological properties.
Polymer Journal (2017) **49,** 189–195; doi:10.1038/pj.2016.94; published online 19 October 2016

INTRODUCTION

The self-organization of functional π-conjugated molecules into well-defined supramolecular architectures using noncovalent interactions such as π-π stacking, hydrogen bonding and solvophobic interactions has received a great deal of attention in various scientific fields, ranging from biological chemistry[1–6] to material science.[7–13] Among the various supramolecular architectures, one-dimensional fibrillar structures are of particular importance, with application to nanowires, gels and biomimetic nanomaterials.[14–16] Such one-dimensional supramolecular nanomaterials are effectively constructed through the stacking of disc-shaped molecules with expanded π-conjugated systems.[17,18] Because of the large π-surface of such molecules, a considerable overlap of π-orbitals between the adjacent molecules is anticipated upon their stacking, which enables the transportation of charge carriers that is promising for applications in organic optoelectronic devices such as organic solar cells and field effect transistors.[19,20] In addition to disc-shaped molecules, multi-arm π-conjugated molecules where three or more π-conjugated units are linked to a central core unit are useful building blocks for constructing one-dimensional supramolecular nanomaterials.[21,22] Although this molecular design has merits, such as its applicability to known functional π-conjugated molecules, it is challenging to introduce many arms onto a central unit because the synthesis and purification of the desired multi-arm products from incomplete side products are demanding.[23] An alternative approach towards such multi-arm π-conjugated structures would be supramolecular macrocyclization (supermacrocyclization) of π-conjugated building blocks using directional noncovalent interactions such as hydrogen-bonding.[24–29] By using this approach, we may obtain a complex architecture of one-dimensionally stacked supermacrocyclic π-conjugated systems with a high degree of internal order.

As a promising molecular design in line with the above approach, we previously reported a naphthalene compound with a barbituric acid hydrogen bonding unit and an aliphatic dendritic unit.[30,31] Atomic force microscopy (AFM), UV–Vis and fluorescence spectroscopic analyses revealed that this naphthalene compound forms cylindrical supramolecular polymers with naphthalene chromophores stacked in a face-to-face (H-type) arrangement. X-ray diffraction analysis revealed that these cylindrical supramolecular polymers are formed by the stacking of hydrogen-bonded hexameric supermacrocycles, referred to here as 'rosettes.' This unique self-organization of naphthalene units is believed to arise from the windmill-like geometry of the rosettes by twisting the naphthalene moieties with respect to the barbituric acid supermacrocyclic plane. Due to this twisting, the rosettes can stack with rotational displacement to afford highly ordered cylindrical nanostructures wherein naphthalene chromophores stack helically in a H-type arrangement. These findings motivated us to explore the self-assembly of compounds with more extended π-conjugated systems but with the same molecular design to gain insight into the relationship of

Department of Applied Chemistry and Biotechnology, Graduate School of Engineering, Chiba University, Chiba, Japan
Correspondence: Professor S Yagai, Department of Applied Chemistry and Biotechnology, Graduate School of Engineering, Chiba University, 1-33 Yayoi-cho, Inage-ku, Chiba 263-8522, Japan.
E-mail: yagai@faculty.chiba-u.jp
Received 15 July 2016; revised 23 August 2016; accepted 25 August 2016; published online 19 October 2016

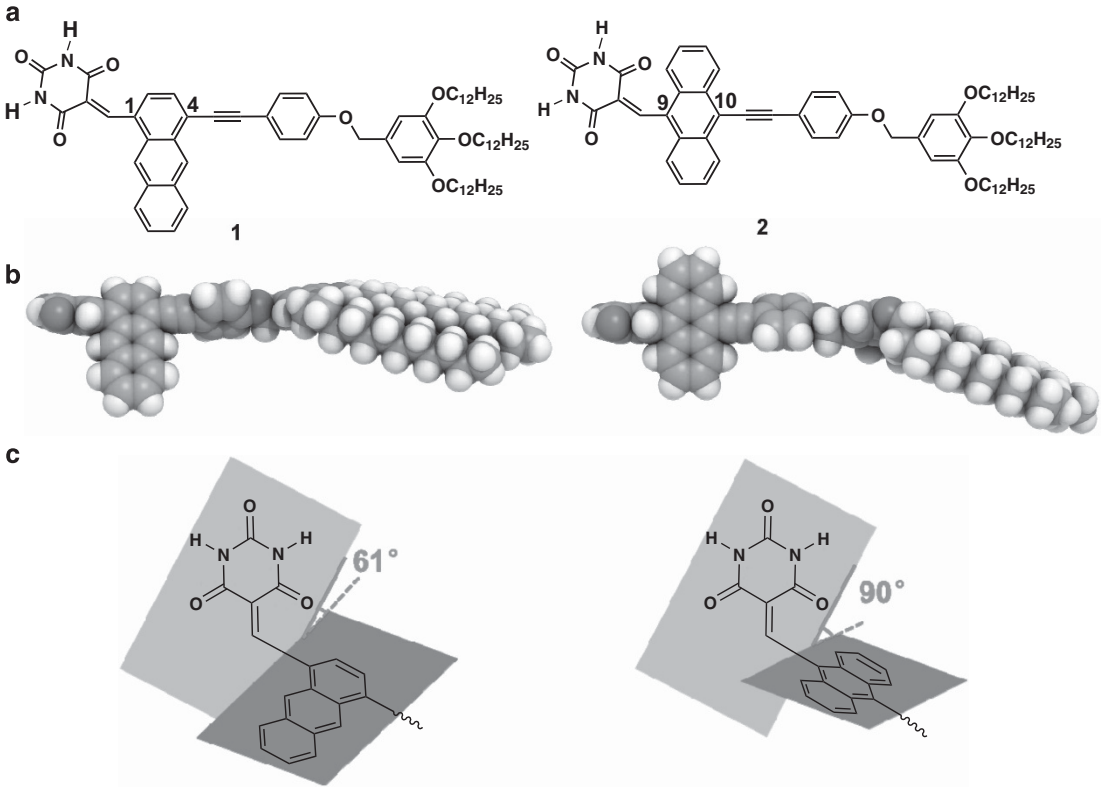

Figure 1 (**a**) Molecular structures and (**b**) geometry-optimized structures (side view) of **1** (left) and **2** (right). (**c**) Schematic representation of different twisting angles of the anthracene chromophore of **1** (left) and **2** (right) with respect to the barbituric acid plane. A full color version of this figure is available at *Polymer Journal* online.

molecular structure to self-assembled morphology and to enhance the functionality of the resulting self-assembled nanostructures.

In this study, we replaced the previous naphthalene unit with an anthracene chromophore because of its more extended π-surface and enriched photophysical properties. We thus designed and synthesized two regioisomeric anthracene-cored barbituric acid compounds (Figure 1a). Molecular modeling showed that the different substitution positions for the barbituric acid moiety on the anthracene core induce different twisting angles between the functional units. We anticipated that this difference would result in different stacking arrangements of the resulting supermacrocycles, leading to the formation of extended supramolecular polymers with different morphological and absorption properties.

RESULTS AND DISCUSSION

Design and synthesis

We designed two regioisomeric anthracene-cored π-conjugated molecules with barbituric acid and a phenylethynyl unit bearing an aliphatic wedge.[32] These functional units were introduced into the anthracene chromophore at the C-1/C-4 positions for **1** and C-9/C-10 positions for **2**, respectively. Compounds **1** and **2** were synthesized according to Supplementary Scheme S1. All intermediates and final products were isolated in good yield and their structures were characterized by ^{1}H, ^{13}C NMR and ESI-MS (see Supplementary Information). Molecular modeling showed that the anthracene chromophores are highly twisted with respect to the barbituric acid plane and the degree of twisting varied significantly with the substituted position at the anthracene chromophore, that is, 61° for the C-1 position in **1**, and almost orthogonal (90°) for the C-9 position in **2** (Figure 1b and c). This conformational difference can be ascribed to the steric repulsion of anthracene aromatic protons with adjacent carbonyl groups and the olefinic proton of the barbituric acid moiety. This conformational difference is expected to induce different stacking arrangements of the hydrogen-bonded rosettes.

Spectroscopic studies

The self-assembly of **1** and **2** was studied in MCH, which is a nonpolar solvent. At 363 K, the UV–Vis absorption spectra of MCH solutions of both compounds ($c = 2.5 \times 10^{-5}$ M) showed two separate absorption bands: one at 330–430 nm and the other in the 440–600 nm region (red curves in Figure 2a and b). These absorption bands could be assigned to the electronic transitions of the transition dipole moments along the short (anthracene long axis) and long axes (anthracene short axis) of the molecularly dissolved species, respectively.[33] The absorption spectra of monomeric species differed such that the absorption bands of **2** are vibronically more structured, due to the differences in electronic delocalization around the anthracene chromophore that arise from differences in the substitution pattern.

Upon cooling the hot monomeric solutions to 293 K, the two regioisomers showed different aggregation-induced spectral changes, which suggests different stacking arrangements of the π-conjugated systems. For **1**, a hypochromic effect of the two absorption bands was observed together with a slight hypsochromic shift (~7 nm) of the longer wavelength band (Figure 2a). This spectral change implies that the π-conjugated units of **1** stack in a face-to-face arrangement, typically classified as H-type stacking (Figure 2c).[34,35] For **2**, in contrast, the absorption band corresponding to the electronic transitions of the transition dipole moment along the molecular long axis displayed a pronounced bathochromic shift of 40 nm with the growth of a new shoulder band at 610 nm. This spectral change

suggests a slipped-stacking arrangement typically classified as J-type stacking.[36–39] However, the absorption band attributed to the electronic transitions of the transition dipole moment along the short molecular axis (anthracene long axis) showed only a hypochromic effect (Figure 2b). The overall spectral change in **2** indicates that this compound stacks with a translational displacement along the long molecular axis while retaining some degree of π-orbital overlap between the anthracene chromophores (Figure 2d).

The presence of extended aggregates in the cooled MCH solutions was established by dynamic light scattering measurements. The MCH solutions ($c = 1 \times 10^{-5}$ M) of the regioisomers exhibited a broad size distribution, in the range of 100–500 nm. The size distribution increased with increasing concentration (Supplementary Figure S1), which suggests the formation of open-ended polymeric aggregates.[30]

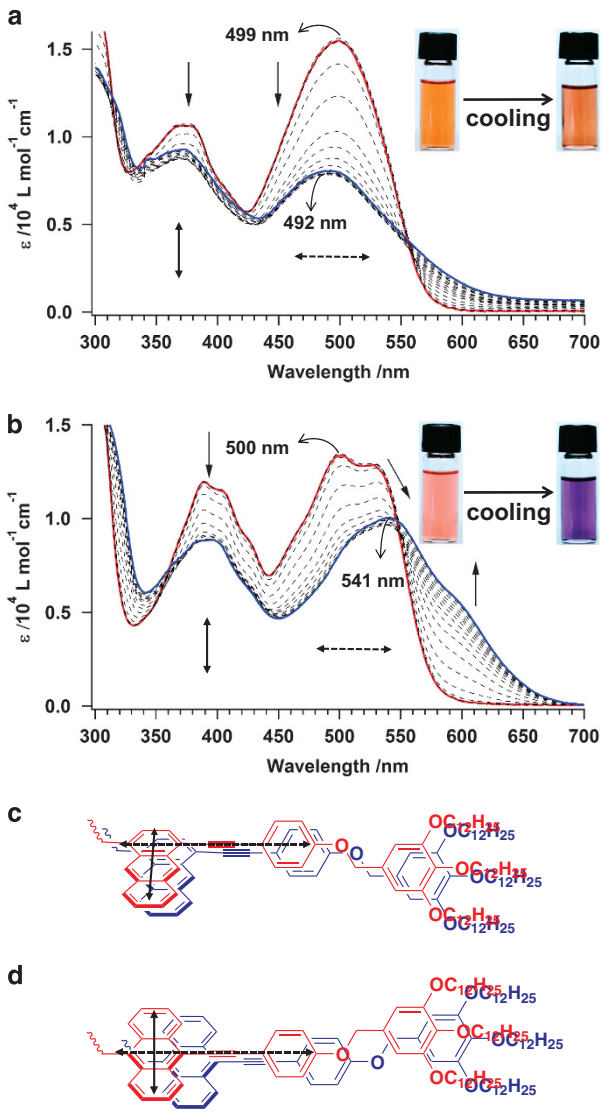

Figure 2 Temperature-dependent UV–Vis spectra of (**a**) **1** and (**b**) **2** measured at a concentration of 2.5×10^{-5} M in MCH. The spectra were recorded upon cooling from 363 K (red line) to 293 K (blue line) at 5 K intervals. The arrows indicate changes upon cooling. Insets in (**a**) and (**b**) show photographs of the aggregated solutions of **1** and **2**, respectively. Schematic representation of proposed stacking arrangement of (**c**) **1** and (**d**) **2**. Double-headed arrows indicate the orientation of the transition dipole moments responsible for the two bands in the absorption spectra.

Noting the fruitful aggregation-induced absorption changes of the regioisomers, we further studied the aggregation process by monitoring spectral changes as a function of temperature upon cooling the MCH solutions ($c = 2.5 \times 10^{-5}$ M) from 373 K to 293 K at a rate of 1 K min^{-1}.[40] When the degree of aggregation (α) calculated from the absorption coefficient at $\lambda = 585$ nm for **1** and $\lambda = 600$ nm for **2** was plotted against temperature, we obtained nonsigmoidal cooling curves, wherein aggregation was abruptly initiated at a critical temperature (green curves in Figure 3a and b). Such a phase transition from molecularly dissolved species to completely aggregated species by lowering temperature is indicative of a cooperative aggregation process, which is typically observed for molecular building blocks possessing more than two specific interactive units (that is, hydrogen bonding and π-π stacking units).[41–43] The cooling curves could be fitted well using the cooperative nucleation-elongation model proposed by Meijer, Schenning and co-workers to give the relevant thermodynamic parameters such as enthalpy change and the association constant (Supplementary Figure S2 and Supplementary Table S1). However, these compounds showed a thermal hysteresis upon subsequent heating (blue curves in Figure 3a and b). Furthermore, the higher temperature region in the heating curves involves a spectral transition that cannot be attributed to dissociation but can be ascribed to a thermal conformational change of monomers. Hence, we did not perform any quantitative fitting analysis of the experimental data.

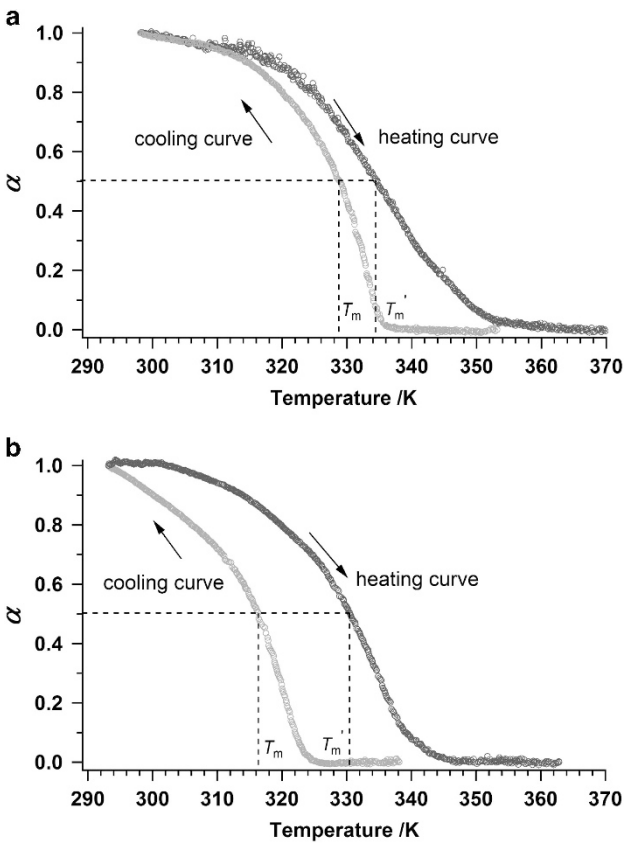

Figure 3 Temperature-dependent fraction of aggregates (α) calculated from apparent absorption intensity at (**a**) $\lambda = 585$ nm for **1** ($c = 2.5 \times 10^{-5}$ M) and (**b**) $\lambda = 600$ nm for **2** ($c = 2.5 \times 10^{-5}$ M) in the cooling and heating process at a rate of 1 K min^{-1}. A full color version of this figure is available at *Polymer Journal* online.

Heating curves show that aggregates of the regioisomers have similar melting temperatures (T_m'), defined as the temperature at which the degree of aggregation (α) is 0.5 ($T_m' = 334$ K for **1** and 330 K for **2**). This indicates comparable thermodynamic stabilities. In contrast, T_m measured from the cooling curve differed greatly between **1** (329 K) and **2** (316 K), and regioisomer **2** exhibited larger thermal hysteresis ($\Delta T_m = T_m' - T_m = 14$ K) compared with regioisomer **1** ($\Delta T_m = 5$ K). This finding indicates that the supramolecular polymerization of **2** is more kinetically controlled than **1**. These observations reveal that conformational differences in the anthracene chromophore greatly impact the self-organization of these molecules. Because the anthracene chromophores in regioisomer **2** are arranged in an orthogonal conformation with respect to the rosette (hexamerized barbituric acids) plane, the π-π stacking interaction operates perpendicular to the stacking direction of rosettes. Such an arrangement is unfavorable for the stacking of rosettes and thereby increases the energy barrier for the nucleation process. Extended supramolecular polymerization through effective π-π stacking interactions thus requires the conformational reorganization of the anthracene core within the rosettes, which in turn causes a large thermal hysteresis between cooling (polymerization) and heating (depolymerization) processes. In contrast, the smaller twisting angle of the anthracene chromophore in **1** makes the geometrical reorganization of their rosettes smaller upon stacking, causing a smaller degree of hysteresis.

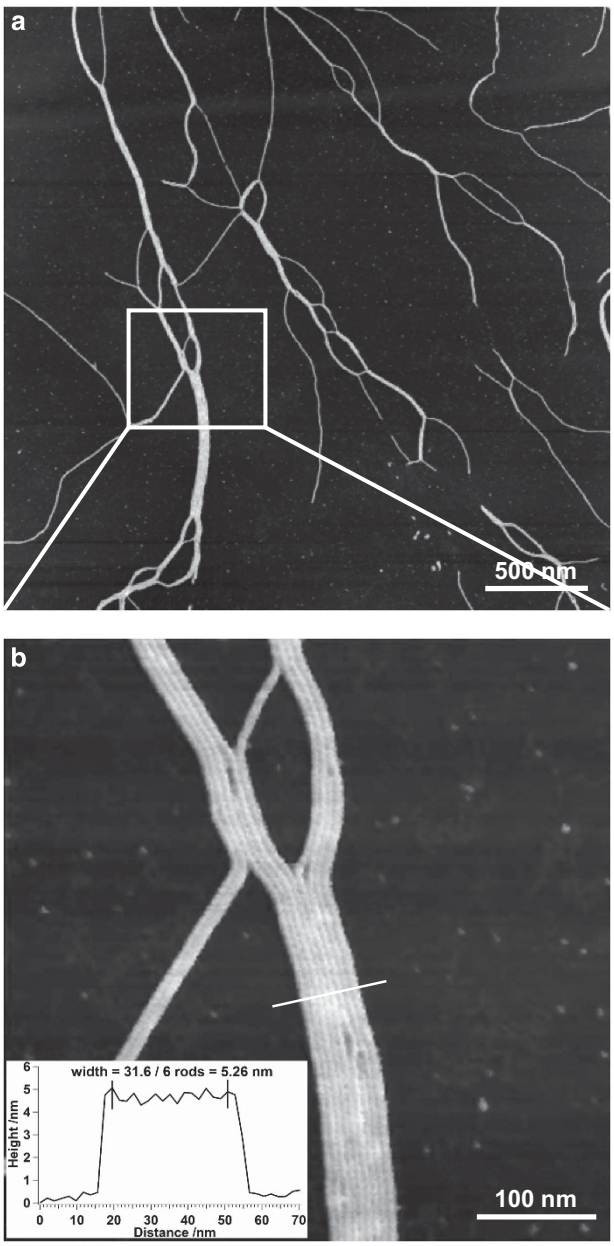

Figure 4 (**a**) AFM height image of **1** ($c = 1 \times 10^{-4}$ M) spin-coated from MCH onto HOPG. (**b**) Enlarged image from (**a**). Inset shows cross-sectional analysis along the white line in (**b**). A full color version of this figure is available at *Polymer Journal* online.

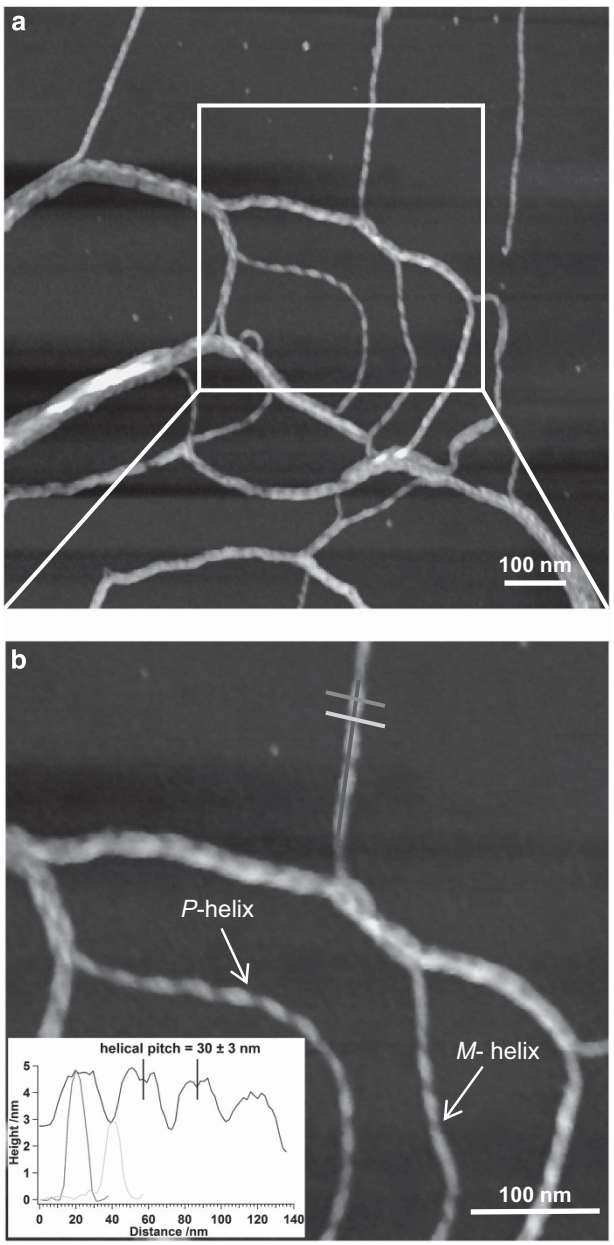

Figure 5 (**a**) AFM height image of **2** ($c = 1 \times 10^{-4}$ M) spin-coated from MCH onto HOPG. (**b**) Enlarged image from (**a**). Inset shows cross-sectional analysis along the red, green and blue lines in (**b**). A full color version of this figure is available at *Polymer Journal* online.

Morphological studies

The morphologies of the aggregates of **1** and **2** were studied by AFM. The samples for AFM measurements were prepared by spin-coating the aggregate solutions ($c = 1 \times 10^{-4}$ M) onto freshly cleaved highly oriented pyrolytic graphite (HOPG). For **1**, well-defined cylindrical nanofibers several micrometers in length were observed (Figure 4a). Cross-sectional analysis of the nanofibers demonstrated that the average thickness was 4.8 ± 0.2 nm. For bundled nanofibers, the average top-to-top distance between the neighboring nanofibers was found to be 5.3 ± 0.2 nm (inset in Figure 4b). The latter value is more reliable because the nanofibers can undergo deformation during solvent evaporation due to adsorption on the substrate surface. These values are considerably shorter than the estimated diameter (8.1 nm) of a molecularly modeled hexameric rosette with extended alkyl chains (Figure 6a). The substantial difference between the top-to-top distance between the neighboring nanofibers and the estimated diameter might be explained by interdigitation of aliphatic wedge units between the stacked rosettes.

Interestingly, for **2**, isolated helically twisted nanofibers[44–48] were visualized by AFM, although most fibers are three-dimensionally bundled (Figure 5a). The helical nanofibers show both *P* and *M* helicity (Figure 5b), which is reasonable because the monomer is intrinsically achiral. Helical pitches are uniform 30 ± 3 nm (Inset in Figure 5b), indicating that the helical structures originate from specific molecular packing. Assuming an intracolumnar distance of 0.35 nm between the neighboring rosettes, one helical pitch corresponds to a stack of 85 rosettes. The thicker parts (brighter parts in AFM; green line in Figure 5b) of the helical structures are 4.0 ± 0.5 nm thick and thinner parts (darker parts; blue line in Figure 5b) are 2.5 ± 0.2 nm thick. The latter value is considerably shorter than the estimated diameter (8.1 nm) of a molecularly modeled hexameric rosette with extended alkyl chains (Figure 6c), indicating a tilted stacking of rosettes to form a column with an ellipsoidal cross-section.[49]

On the basis of the above observations, we propose a mechanism for the formation of supramolecular polymers by **1** and **2**. Because of the twisted conformation of anthracene chromophores, the rosettes of both regioisomers take on a crown gear-like morphology.[30] In case of **1**, π-π stacking interactions between the anthracene chromophores can be achieved by the rotational displacement of the rosettes due to their smaller twisting angle with respect to the rosette plane (Figure 6b). In contrast, in case of **2**, the π-π stacking interaction between the anthracene chromophores is not feasible via simple rotational displacement of the rosettes due to their large twisting angle. Hence, they must undergo both rotational and lateral displacement thereby arranging the long axis of the molecules in a J-type manner between the stacked rosettes. In this arrangement, anthracene chromophores may be stacked in a herringbone-type arrangement, consistent with the hypochromic effect of the absorption band (Figure 2b). This local packing arrangement of the rosettes would lead to a helical morphology upon extended supramolecular polymerization (Figure 6d).

Influence of chiral solvent

We further investigated the helical morphology observed for the aggregates of **2** with the addition of small amounts of chiral solvents. It is known that certain chiral solvents can bias the handedness of helical stacks.[50] Here, we attempted to transfer the point chirality of (*R*)-limonene as a chiral cosolvent to the supramolecular chirality of helical rosette stacks of **2**. UV–Vis absorption spectra of aggregates of **2** ($c = 2.5 \times 10^{-5}$ M) in MCH:(*R*)-limonene mixtures with a varying volume fraction of (*R*)-limonene showed a gradual red shift in the absorption maximum, accompanied by an increase in the absorption intensity at 610 nm. The spectral changes showed a maximum red shift of 15 nm at 20% (*R*)-limonene fraction compared with a pure MCH solution. Upon further increase, the (*R*)-limonene fraction resulted in a reduction in intensity in the shoulder band at 610 nm. The UV–Vis spectrum eventually became similar to the absorption

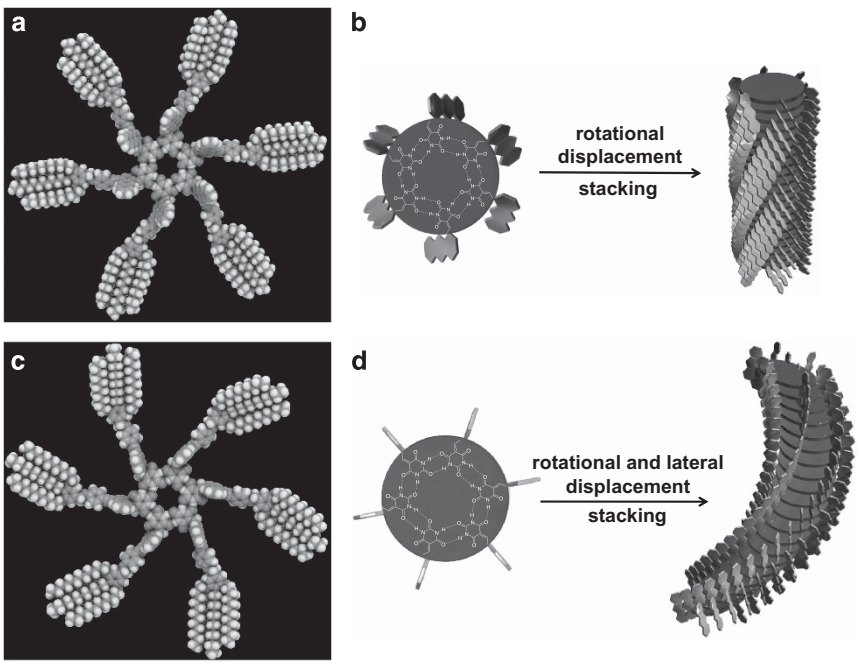

Figure 6 Geometry-optimized structure of hexameric rosettes and schematic representation of hierarchical organization of rosettes of **1** (**a** and **b**) and **2** (**c** and **d**). A full color version of this figure is available at *Polymer Journal* online.

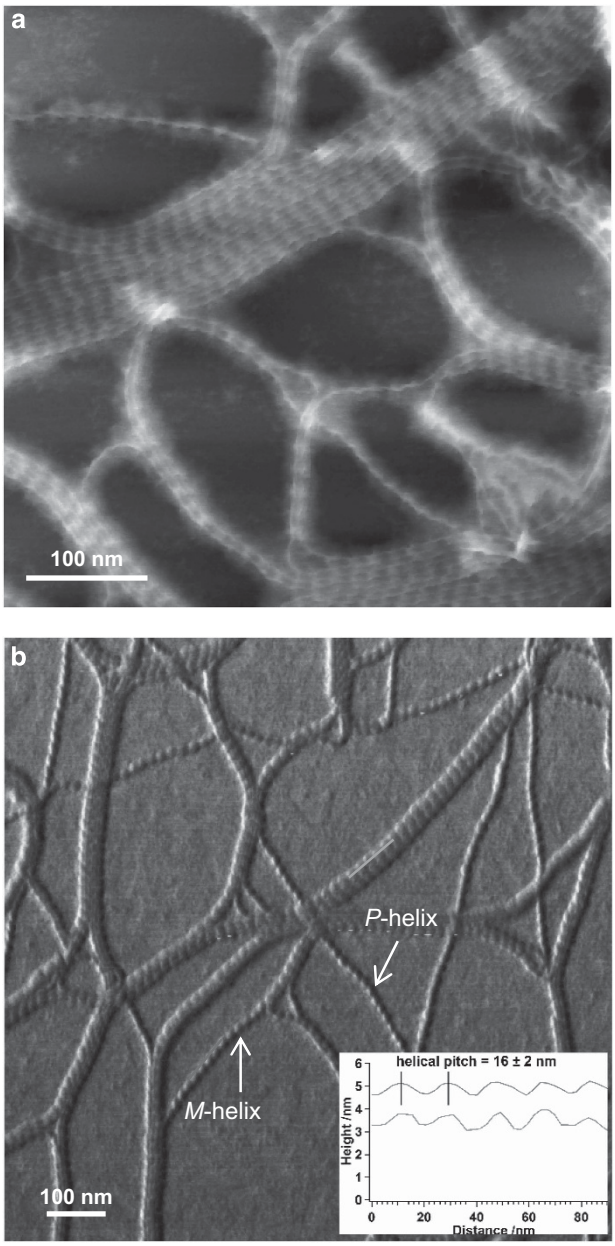

Figure 7 (**a**) AFM height image of **2** spin-coated from a MCH:(*R*)-limonene mixture (80:20 v/v%; $c = 1 \times 10^{-4}$ M) onto HOPG. (**b**) Tapping-mode phase image of **2**. Inset shows cross sectional analysis along the red and green lines in (**b**). A full color version of this figure is available at *Polymer Journal* online.

spectrum of the monomeric species in MCH at higher temperatures for limonene fractions above 50%, indicating the disassembly of the aggregates (Supplementary Figure S3a). Overall, this finding indicates that at lower solvent ratios, (*R*)-limonene unexpectedly has an impact on the π–π stacking of π-conjugated units of **2**. The more prominent spectral feature associated with J-type stacking implies that, a more ordered stacking of rosettes with a larger offset is achieved by adding small amounts of (*R*)-limonene. Despite this positive change in the absorption spectra from (*R*)-limonene, the solution showed no circular dichroism activity, even upon changing the ratio of (*R*)-limonene and MCH (Supplementary Figure S3b).

Although we could not induce supramolecular chirality in the nanofibers, the use of limonene as a cosolvent suppressed the 3D bundling of helical fibers, and all helical fibers observed were two-dimensionally aligned on the HOPG surface upon drying (Figure 7a and Supplementary Figure S4). However, the image resolution does not allow us to assign the handedness of helicity. Hence, to image helical structures more clearly, we analyzed the aligned fibers by means of phase imaging in AFM (see Supplementary Information). Although the average height of the helical nanofibers (3.7 ± 0.5 nm) is comparable to those formed in pure MCH, cross-sectional analysis along the long axis of the nanofibers revealed a much-reduced helical pitch of 16 ± 2 nm compared with those obtained in pure MCH (inset in Figure 7b). This finding demonstrates that (*R*)-limonene causes a larger rotational displacement of rosettes within the fiber. Such a change in rotational displacement can affect the π–π stacking arrangement, as reflected in the UV–Vis results, wherein a larger red shift in absorption maxima was observed in the presence of limonene. An identical effect was also observed when (*S*)-limonene was used as a cosolvent (Supplementary Figure S5 and S6). In contrast, this effect from limonene was not observed for cylindrical nanofibers of **1** (Supplementary Figure S7 and S8), which further confirms that **1** is already tightly packed in the optimal stacking geometry of the rosettes in MCH.

CONCLUSION

We have synthesized two regioisomeric anthracene-cored self-assembling barbituric acid compounds. The regiomeric introduction of barbituric acid and aliphatic tail units onto anthracene cores resulted in distinctly different π–π stacking arrangements upon aggregation in nonpolar solvent. As a result, both regioisomers self-assemble to form supramolecular polymers with either non-helical or helically twisted fibrous morphologies. The formation of these fibrous nanoaggregates can be rationalized by the formation of hydrogen-bonded hexameric rosettes, and the distinct π–π stacking arrangements are attributed to conformational differences in the anthracene chromophores with respect to the plane of the rosettes. This type of rational strategy to simultaneously control chromophore packing arrangements and self-assembled nanoarchitectures are promising for the design and synthesis of organic functional nanomaterials with specific physical properties.

CONFLICT OF INTEREST

The authors declare no conflict of interest.

ACKNOWLEDGEMENTS

This work was supported by KAKENHI (no. 26102010) and a Grant-in-Aid for Scientific Research on Innovative Areas in 'π-Figuration' (no. 26102001) by the The Ministry of Education, Culture, Sports, Science and Technology, Japan.

1 Lehn, J.-M. *Supramolecular Chemistry*, Concepts and Perspectives (John Wiley & Sons, Ltd., Germany, 1995).
2 Zelzer, M. & Ulijn, R. V. Next-generation peptide nanomaterials: molecular networks, interfaces and supramolecular functionality. *Chem. Soc. Rev.* **39**, 3351–3357 (2010).
3 Boekhoven, J. & Stupp, S. I. 25th anniversary article: supramolecular materials for regenerative medicine. *Adv. Mater.* **26**, 1642–1659 (2014).
4 Wang, D., Tong, G., Dong, R., Zhou, Y., Shen, J. & Zhu, X. Self-assembly of supramolecularly engineered polymers and their biomedical applications. *Chem. Commun.* **50**, 11994–12017 (2014).
5 Pires, R. A., Abul-Haija, Y. M., Costa, D. S., Novoa-Carballal, R., Reis, R. L., Ulijn, R. V. & Pashkuleva, I. Controlling cancer cell fate using localized biocatalytic self-assembly of an aromatic carbohydrate amphiphile. *J. Am. Chem. Soc.* **137**, 576–579 (2015).

6 Boekhoven, J., Helen Zha, R., Tantakitti, F., Zhuang, E., Zandi, R., Newcomb, C. J. & Stupp, S. I. Alginate-peptide amphiphile core-shell microparticles as a targeted drug delivery system. *RSC. Adv.* **5**, 8753–8756 (2015).
7 Schenning, A. P. H. J. & Meijer, E. W. Supramolecular electronics; nanowires from self-assembled π-conjugated systems. *Chem. Commun.* 3245–3258 (2005).
8 Palmer, L. C. & Stupp, S. I. Molecular self-assembly into one-dimensional nanostructures. *Acc. Chem. Res.* **41**, 1674–1684 (2008).
9 Zang, L., Che, Y. & Moore, J. S. One-dimensional self-assembly of planar π-conjugated molecules: adaptable building blocks for organic nanodevices. *Acc. Chem. Res.* **41**, 1596–1608 (2008).
10 Aida, T., Meijer, E. W. & Stupp, S. I. Functional supramolecular polymers. *Science* **335**, 813–817 (2012).
11 Treier, M., Liscio, A., Mativetsky, J. M., Kastler, M., Müllen, K., Palermo, V. & Samorì, P. Photoconductive and supramolecularly engineered organic field-effect transistors based on fibres from donor-acceptor dyads. *Nanoscale* **4**, 1677–1681 (2012).
12 Babu, S. S., Praveen, V. K. & Ajayaghosh, A. Functional π-gelators and their applications. *Chem. Rev.* **114**, 1973–2129 (2014).
13 Weingarten, A. S., Kazantsev, R. V., Palmer, L. C., McClendon, M., Koltonow, A. R., Samuel, A. P. S., Kiebala, D. J., Wasielewski, M. R. & Stupp, S. I. Self-assembling hydrogel scaffolds for photocatalytic hydrogen production. *Nat. Chem.* **6**, 964–970 (2014).
14 Würthner, F., Saha-Möller, C. R., Fimmel, B., Ogi, S., Leowanawat, P. & Schmidt, D. Perylene bisimide dye assemblies as archetype functional supramolecular materials. *Chem. Rev.* **116**, 962–1052 (2016).
15 Webber, M. J., Appel, E. A., Meijer, E. W. & Langer, R. Supramolecular biomaterials. *Nat. Mater.* **15**, 13–26 (2016).
16 Ghosh, S., Praveen, V. K. & Ajayaghosh, A. The chemistry and applications of π-gels. *Annu. Rev. Mater. Res.* **46**, 235–262 (2016).
17 Sergeyev, S., Pisula, W. & Geerts, Y. H. Discotic liquid crystals: a new generation of organic semiconductors. *Chem. Soc. Rev.* **36**, 1902–1929 (2007).
18 Kumar, S. Playing with discs. *Liq. Cryst.* **36**, 607–638 (2009).
19 Laschat, S., Baro, A., Steinke, N., Giesselmann, F., Hägele, C., Scalia, G., Judele, R., Kapatsina, E., Sauer, S., Schreivogel, A. & Tosoni, M. Discotic liquid crystals: from tailor-made synthesis to plastic electronics. *Angew. Chem. Int. Ed.* **46**, 4832–4887 (2007).
20 Kaafarani, B. R. Discotic liquid crystals for opto-electronic applications. *Chem. Mater.* **23**, 378–396 (2011).
21 Lehmann, M. Star mesogens (hekates)—tailor-made molecules for programming supramolecular functionality. *Chem. Eur. J.* **15**, 3638–3651 (2009).
22 Kanibolotsky, A. L., Perepichka, I. F. & Skabara, P. J. Star-shaped π-conjugated oligomers and their applications in organic electronics and photonics. *Chem. Soc. Rev.* **39**, 2695–2728 (2010).
23 Nierle, J., Barth, D. & Kuck, D. Pentakis(phenylethynyl)benzene and hexakis (phenylethynyl)benzene: a revision concerning two far too similar prototype hydrocarbons. *Eur. J. Org. Chem.* **4**, 867–872 (2004).
24 Kato, T., Yasuda, T., Kamikawa, Y. & Yoshio, M. Self-assembly of functional columnar liquid crystals. *Chem. Commun.* 729–739 (2009).
25 Yagai, S. Supramolecularly engineered functional π-assemblies based on complementary hydrogen-bonding interactions. *Bull. Chem. Soc. Jpn.* **88**, 28–58 (2015).
26 Yagai, S., Suzuki, M., Lin, X., Gushiken, M., Noguchi, T., Karatsu, T., Kitamura, A., Saeki, A., Seki, S., Kikkawa, Y., Tani, Y. & Nakayama, K. Supramolecular engineering of oligothiophene nanorods without insulators: hierarchical association of rosettes and photovoltaic properties. *Chem. Eur. J.* **20**, 16128–16137 (2014).
27 Yagai, S., Usui, M., Seki, T., Murayama, H., Kikkawa, Y., Uemura, S., Karatsu, T., Kitamura, A., Asano, A. & Seki, S. Supramolecularly engineered perylene bisimide assemblies exhibiting thermal transition from columnar to multilamellar structures. *J. Am. Chem. Soc.* **134**, 7983–7994 (2012).
28 Yagai, S., Aonuma, H., Kikkawa, Y., Kubota, S., Karatsu, T., Kitamura, A., Mahesh, S. & Ajayaghosh, A. Rational design of nanofibers and nanorings through complementary hydrogen-bonding interactions of functional π systems. *Chem. Eur. J.* **16**, 8652–8661 (2010).
29 Jonkheijm, P., Miura, A., Zdanowska, M., Hoeben, F. J. M., De Feyter, S., Schenning, A. P. H. J., De Schryver, F. C. & Meijer, E. W. π-conjugated oligo-(π-phenylenevinylene) rosettes and their tubular self-assembly. *Angew. Chem. Int. Ed.* **43**, 74–78 (2004).
30 Yagai, S., Goto, Y., Lin, X., Karatsu, T., Kitamura, A., Kuzuhara, D., Yamada, H., Kikkawa, Y., Saeki, A. & Seki, S. Self-organization of hydrogen-bonding naphthalene chromophores into J-type nanorings and H-type nanorods: impact of regioisomerism. *Angew. Chem. Int. Ed.* **51**, 6643–6647 (2012).
31 Aratsu, K., Prabhu, D. D., Iwawaki, H., Lin, X., Yamauchi, M., Karatsu, T. & Yagai, S. Self-sorting regioisomers through the hierarchical organization of hydrogen-bonded rosettes. *Chem. Commun.* **52**, 8211–8214 (2016).
32 Rosen, B. M., Wilson, C. J., Wilson, D. A., Peterca, M., Imam, M. R. & Percec, V. Dendron-mediated self-assembly, disassembly, and self-organization of complex systems. *Chem. Rev.* **109**, 6275–6540 (2009).
33 Levitus, M. & Garcia-Garibay, M. A. Polarized electronic spectroscopy and photophysical properties of 9, 10-bis(phenylethynyl)anthracene. *J. Phys. Chem. A.* **104**, 8632–8637 (2000).
34 Würthner, F. & Yao, S. Dipolar dye aggregates: a problem for nonlinear optics, but a chance for supramolecular chemistry. *Angew. Chem. Int. Ed.* **39**, 1978–1981 (2000).
35 Prabhu, D. D., Sivadas, A. P. & Das, S. Solvent assisted fluorescence modulation of a C3-symmetric organogelator. *J. Mater. Chem. C.* **2**, 7039–7046 (2014).
36 Jelley, E. E. Spectral absorption and fluorescence of dyes in the molecular state. *Nature* **138**, 1009–1010 (1936).
37 Yagai, S., Seki, T., Karatsu, T., Kitamura, A. & Würthner, F. Transformation from H- to J-aggregated perylene bisimide dyes by complexation with cyanurates. *Angew. Chem. Int. Ed.* **47**, 3367–3371 (2008).
38 Würthner, F., Kaiser, T. E. & Saha-Möller, C. R. J-aggregates: from serendipitous discovery to supramolecular engineering of functional dye materials. *Angew. Chem. Int. Ed.* **50**, 3376–3410 (2011).
39 Yagai, S., Nakano, Y., Seki, S., Asano, A., Okubo, T., Isoshima, T., Karatsu, T., Kitamura, A. & Kikkawa, Y. Supramolecularly engineered aggregation of a dipolar dye: vesicular and ribbon like architectures. *Angew. Chem. Int. Ed.* **49**, 9990–9994 (2010).
40 Smulders, M. M. J., Nieuwenhuizen, M. M. L., de Greef, T. F. A., van der Schoot, P., Schenning, A. P. H. J. & Meijer, E. W. How to distinguish isodesmic from cooperative supramolecular polymerisation. *Chem. Eur. J.* **16**, 362–367 (2010).
41 Zhao, D. & Moore, J. S. Nucleation-elongation: a mechanism for cooperative supramolecular polymerization. *Org. Biomol. Chem.* **1**, 3471–3491 (2003).
42 Jonkheijm, P., van der Schoot, P., Schenning, A. P. H. J. & Meijer, E. W. Probing the solvent-assisted nucleation pathway in chemical self-assembly. *Science* **313**, 80–83 (2006).
43 Rest, C., Kandanelli, R. & Fernández, G. Strategies to create hierarchical self-assembled structures via cooperative non-covalent interactions. *Chem. Soc. Rev.* **44**, 2543–2572 (2015).
44 Hill, J. P., Jin, W., Kosaka, A., Fukushima, T., Ichihara, H., Shimomura, T., Ito, K., Hashizume, T., Ishii, N. & Aida, T. Self-assembled hexa-peri-hexabenzocoronene graphitic nanotube. *Science* **304**, 1481–1483 (2004).
45 Ajayaghosh, A., Vijayakumar, C., Varghese, R. & George, S. J. Cholesterol-aided supramolecular control over chromophore packing: twisted and coiled helices with distinct optical, chiroptical, and morphological features. *Angew. Chem. Int. Ed.* **118**, 470–474 (2006).
46 Li, X., Stepanenko, V., Chen, Z., Prins, P., Siebbeles, L. D. A. & Würthner, F. Functional organogels from highly efficient organogelator based on perylene bisimide semiconductor. *Chem. Commun.* 3871–3873 (2006).
47 Huang, Z., Kang, S., Banno, M., Yamaguchi, T., Lee, D., Seok, C., Yashima, E. & Lee, M. Pulsating tubules from noncovalent macrocycles. *Science* **337**, 1521–1526 (2012).
48 Yamauchi, M., Ohba, T., Karatsu, T. & Yagai, S. Photoreactive helical nanoaggregates exhibiting morphology transition on thermal reconstruction. *Nat. Commun.* **6**, 8936 (2015).
49 Ouchi, H., Lin, X., Kizaki, T., Prabhu, D. D., Silly, F., Kajitani, T., Fukushima, T., Nakayama, K. & Yagai, S. Hydrogen-bonded oligothiophene rosettes with a benzodithiophene terminal unit: self-assembly and application to bulk heterojunction solar cells. *Chem. Commun.* **52**, 7874–7877 (2016).
50 George, S. J., Tomović, Z., Schenning, A. P. H. J. & Meijer, E. W. Insight into the chiral induction in supramolecular stacks through preferential chiral solvation. *Chem. Commun.* **47**, 3451–3453 (2011).

Supplementary Information accompanies the paper on Polymer Journal website (http://www.nature.com/pj)